Title
Using Heat as a Predictor of CO2 Breakthrough in Highly Heterogeneous Reservoirs

Journal
Geophysical Research Letters, 46(11)

ISSN
0094-8276

Authors
Jayne, Richard S
Zhang, Yingqi
Pollyea, Ryan M

Publication Date
2019-06-16

DOI
10.1029/2019gl083362

Peer reviewed

Using Heat as a Predictor of CO_2 Breakthrough in Highly Heterogeneous Reservoirs

Richard S. Jayne[1], Yingqi Zhang[2], and Ryan M. Pollyea[1]

[1]Department of Geosciences, Virginia Polytechnic Institute and State University, Blacksburg, VA, USA, [2]Energy Geosciences Division, Lawrence Berkeley National Laboratory, Berkeley, CA, USA

Correspondence to: R. S. Jayne, rjayne@vt.edu

Abstract

Injecting supercritical CO_2 into the subsurface changes the temperature, pressure, and geochemistry of the storage reservoir. Understanding these perturbations within the reservoir may be used to monitor the CO_2 plume during a carbon capture and sequestration (CCS) project. Here we analyze results from 1-D, 2-D, and 3-D numerical modeling studies to investigate how the thermal signature of the CO_2-water system evolves during CCS. These models show that the thermodynamic processes of the CO_2-water system results in a characteristic thermal profile within a homogeneous storage reservoir during a CO_2 injection. This thermal signature is characterized by warming front of up to 4 °C, which is caused by CO_2 dissolution and migrates contemporaneously with free-phase CO_2 migration. When reservoir properties are highly heterogeneous, this thermal front travels well ahead of free-phase CO_2, thus implying that thermal monitoring may be an effective predictor of CO_2 breakthrough.

Plain Language Summary

When CO_2 is injected into a geologic reservoir, it causes the pressure, temperature, and chemical systems with the reservoir to change. Understanding these changes are important in order to plan a CO_2 injection and monitor the CO_2 during the injection. Monitoring CO_2 in the subsurface is required to avoid negative health, safety, and environmental impacts. The temperature effects associated with a CO_2 injection may be used as a way to monitor the CO_2 plume during the injection phase. Results here show that the heat of dissolution can cause temperature to increase up to 4 °C and can be used as a way to predict the arrival of CO_2.

1 Introduction

Heat has been used as a groundwater tracer since Slichter (1905) utilized temperature to show that a pond in Long Island, New York, was infiltrating the local groundwater. Thereafter, studies have utilized heat to study groundwater inflow to lakes (Lee, 1985), identify gaining or losing streams (Conant, 2004), quantify seasonal variations in the shallow subsurface (Storey et al., 2003), characterize flow through fractures (Bodvarsson, 1969), quantify fracture attributes in hydrothermal systems (Anderson & Fairley, 2008; Heffner & Fairley, 2006), and identify flow patterns in groundwater basins (Bachu, 1988). More recently, thermal tracers have been utilized to

characterize fractures and heat transfer within enhanced geothermal systems. For example, Pruess and Doughty (2010) simulate a single-well injection withdrawal test to illustrate the effectiveness of using heat as a tracer within enhanced geothermal systems. This study also highlights the advantages of using heat over chemical tracers because thermal parameters have much less variability than chemical parameters, and thermal diffusivity is 4–5 orders of magnitude larger than the diffusivity of solutes in lower permeability reservoirs. Shook and Suzuki (2017) present an analytical solution to show that temperature is a robust tool to characterize EGS environments. Additionally, Manga (2001) points out the advantages of using heat as a tracer, namely, the ability to collect high-resolution spatial and temporal data.

Numerical models are frequently utilized to study the thermal processes associated with CO_2 storage in geologic reservoirs (André et al., 2010; Han et al., 2010; Hurter et al., 2007; Jayne et al., 2019; Oldenburg, 2007; Pruess, 2005a; Zhao & Cheng, 2017). These studies focus largely on Joule-Thomson cooling that occurs during a CO_2 injection; this refers to the cooling that occurs when a gas, for example, CO_2, expands. For example, Zhang et al. (2011) combines this thermodynamic process with other observations to estimate residual CO_2 saturation based on the difference between water and CO_2 diffusivity. Similarly, Pruess (2005a) models CO_2 flow and phase change within a hypothetical leakage system using idealized faults to investigate the risks associated with geologic storage of CO_2, and Oldenburg (2007) examines adiabatic cooling (Joule-Thomson effect) caused by the decompression of injected CO_2 into a natural gas reservoir. André et al. (2010) investigates the thermal impact a supercritical CO_2 injection has on the reactive nature of a carbonate saline reservoir and shows relatively small cooling effects (1–2 °C), which is similar to the results of Oldenburg (2007).

While the thermodyamics of CO_2 expansion are well known to the carbon capture and sequestration (CCS) community, there have been few studies investigating the thermal effects caused by CO_2 dissolution, that is, heat of dissolution. Thermal monitoring has also been proposed as a method for monitoring CO_2 leakage from a storage reservoir (Zeidouni et al., 2014; Zhang et al., 2018a). Han et al. (2010) and Han et al. (2012) present numerical modeling studies that evaluate the nonisothermal processes associated with a supercritical CO_2 injection into saline formations. These studies suggest that temperature changes during a CO_2 injection may be an essential monitoring tool when temperature changes are greater than 1 °C. However, the temperature changes within the reservoir may not only be caused by CO_2. For example, a recent study of an enhanced geothermal system (EGS) found that the thermodynamic effects associated with H_2O cause an increase in temperature at the production well prior to the arrival of the injected fluid (Zhang et al., 2018b). This thermal anomaly is the result of thermodynamic processes (Joule-Thomson effects) that cause water to

release heat when subject to sharp pressure gradients (Stauffer et al., 2014), as is the case during fluid circulation in EGS systems (Zhang et al., 2018b).

The thermal effects associated with interactions between CO_2 and water have been well studied individually; however, the relationship between reservoir properties (permeability and porosity) and the thermodynamic processes governing fluid temperature remains an open question. Moreover, the influence of spatially heterogeneous reservoir properties on thermal fluid processes has yet to be considered. To fill this gap in knowledge, this study is designed to learn how the fluid temperature signal responds to (i) systematic variations of bulk permeability and porosity and (ii) spatially heterogeneous permeability fields, for example, in a basalt reservoir.

2 Thermal Processes in the CO_2-Water System

Injecting free-phase CO_2 into the subsurface changes the thermal regime by altering the natural conduction and advection of heat and imposing four thermodynamic processes related to the CO_2-water system: (i) Joule-Thomson cooling from CO_2 expansion, (ii) heat released by CO_2 dissolution, (iii) cooling caused by water vaporization (Han et al., 2012), and (iv) Joule-Thomson heating from water expansion. Each of these thermal processes occurs at different locations within and/or around the CO_2 plume, and they are affected by pressure gradients caused by the injection of CO_2 into the storage reservoir. The combination of these effects results in a dynamically changing thermal profile within the storage reservoir over the course of a CCS project.

2.1 Joule-Thomson Effect

The Joule-Thomson effect is the temperature change associated with the expansion or compression of a fluid (i.e., change in pressure), such as CO_2 or H_2O (Roebuck et al., 1942). In the context of this study, Joule-Thomson cooling refers to the cooling associated with the decompression of CO_2 and Joule-Thomson heating refers to the heating caused by the decompression of H_2O. The resulting temperature change (ΔT) due to a pressure change (ΔP) has been derived experimentally under isenthalpic (constant enthalpy) conditions,

$$\mu_{\mathrm{JT}} = \lim_{x \to 0} \left[\frac{\Delta T}{\Delta P}\right]_H = \left[\frac{\delta T}{\delta P}\right]_H \quad (1)$$

where μ_{JT} is the Joule-Thomson coefficient and can be determined by the limiting ratio of ΔT to ΔP under a constant enthalpy (H) (Engel & Reid, 2010). When μ_{JT} is positive, a fluid will heat upon compression and cool upon expansion and vice versa when μ_{JT} is negative. For conditions of interest in CCS ($T \approx$ 30–80 °C and $P \approx$ 10–40 MPa), Han et al. (2010) points out that μ_{JT} for CO_2 is positive, generally increases as T and P decrease, and ranges from 0.125–5 °C/MPa. Conversely, at these same conditions μ_{JT} of H_2O can range from ~0.17–0.22 °C/MPa (NIST, 2018), which results in H_2O heating upon

expansion and cooling upon compression (Stauffer et al., 2014; Zhang et al., 2018b).

2.2 Heat of Dissolution and Vaporization

When supercritical CO_2 is injected into a reservoir, the interface between the CO_2 and reservoir water allows for CO_2 to dissolve in the water and for the water to dissolve into the CO_2. At temperature conditions relevant for CCS, the dissolution of CO_2 into water is an exothermic reaction referred to as *heat of dissolution*. Koschel et al. (2006) provides experimental data on the enthalpy and solubility of CO_2 in water, the enthalpy of solution at 50 °C and pressures from 5–20 MPa is −15.2 kJ/mol and at 100 °C with pressures from 5–20 MPa is −7.9 kJ/mol. As thermal energy is released from this reaction, the surrounding water, CO_2, and reservoir rock experience an increase in temperature. Conversely, water vaporization into the supercritical-phase CO_2 requires the input of energy (positive enthalpy) resulting in cooling of the surrounding water, CO_2, and reservoir rock (Han et al., 2010). While the heat of dissolution and water vaporization are competing processes at the water-CO_2 interface, the solubility of CO_2 in water is $\sim 8.4 \times 10^{-3}$ mole fraction (King & Coan, 1971) and the solubility of water in CO_2 is $\sim 4.0 \times 10^{-4}$ mole fraction (Carroll et al., 1991). Since the solubility of CO_2 in water is 20 times greater than that of water in CO_2, the effects of water vaporization are negligible.

When free-phase CO_2 is pumped into a disposal reservoir, the competing effects of Joule-Thomson cooling (CO_2), Joule-Thomson heating (H_2O), and heat of dissolution result in a dynamically changing thermal profile within the CO_2-water-rock system. This study is designed to (i) quantify the thermal contributions of the Joule-Thomson and heat of dissolution effects during a CO_2 injection scenario, (ii) show how these processes vary with changes in permeability and porosity, and (iii) evaluate the efficacy of thermal monitoring to predict CO_2 breakthrough in reservoirs characterized by homogeneous and highly heterogeneous hydraulic properties.

3 Methods

We implement a numerical modeling study to quantify the thermal structure that develops during a typical CCS scenario. For this scenario, CO_2 is injected at 40 °C for 20 years at a constant rate of 1 kg/s into a reservoir with an initial temperature of 40 °C. The purpose of injecting the CO_2 at the same temperature as the initial reservoir temperature is to isolate the thermophysical effects of a CO_2 injection. We initially characterize the thermal structure of the CO_2-water system using a 1-D simulation ensemble comprising 459 homogeneous reservoirs with unique combinations of permeability and porosity. To analyze how vertical flow affects the thermal profile during a CO_2 injection, we repeat the model scenario by adding vertical discretization to the 1-D model, which results in a 2-D radially symmetric grid. We then consider the effects of reservoir heterogeneity by interrogating the thermal structure of a 3-D CCS simulation that was originally developed by Jayne et al. (2019) to understand the implications of

spatially uncertain permeability distributions during CO_2 injections into flood basalt reservoirs.

The 1-D homogeneous model is conceptualized as a single, radially symmetric layer with 16-m thickness (829- to 845-m depth) and 100-km lateral extent, the latter of which approximates a semi-infinite radial dimension (Figure 1). The injection well comprises a single grid cell with a radius of 0.1 m and represents the inner boundary for the model domain. Beyond the injection well, 949 grid cells are discretized with logarithmically increasing increments (Δr) from 0.1 to 10,000 m. In order to simulate a semi-infinite far-field dimension, an additional 50 grid cells with logarithmically increasing Δr are specified from 10,000 to 100,000 m. The high resolution of the grid near the injection well is chosen to minimize discretization effects that create a non-physical pressure spike in early time (Mathias et al., 2013). Owing to the success of recent CCS pilot projects in highly heterogeneous basalt reservoirs (Matter et al., 2016; McGrail et al., 2017), the initial conditions and hydraulic properties specified for this project are representative of basalt (Pollyea, 2016; Figure 1). Initial conditions are specified as 8.3-MPa fluid pressure, reservoir temperature is 40 °C, and salt concentration is 10,000 ppm, which reproduce conditions encountered within the pilot borehole at the Wallula Basalt Sequestration Pilot Project in southeast Washington State, USA (McGrail et al., 2017).

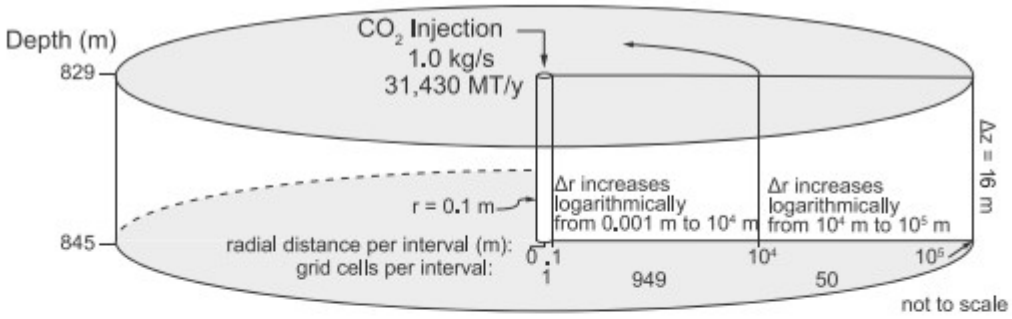

RESERVOIR PARAMETERS

	Relative Permeability	Capillary Pressure
P_f = 8.30 MPa	λ = 0.550	λ = 0.500
T = 40.0 °C	S_{lr} = 0.30	S_{lr} = 0.0
NaCl = 10,000 ppm	S_{ls} = 1.0	α (Pa^{-1}) = 1.39 x 10^{-6}
k = 1.0 × 10^{-13} - 10^{-15} m^2	S_{gr} = 0.25	S_{ls} = 0.999
φ = 0.05 - 0.45		

Figure 1. Schematic illustration and model properties for the 1-D radially symmetric model domain used for this study. The injection well is idealized as a single grid cell with a radius of 0.1 m. The next 949 grid cells increase logarithmically from 0.001 to 10,000 m, another 50 grid cells that increase logarithmically are added to represent semiinfinite lateral dimensions of 100,000 m.

To account for the interfering effects of CO_2 and water occupying the same pore space, we implement the Van Genuchten (1980) constitutive

relationships for relative permeability and capillary pressure. While the multiphase properties of basalt are uncertain, Gran et al. (2017) found that relative permeability is highly interfering. In addition, Pollyea (2016) interrogated the relative permeability parameter space and found that a phase-interference parameter (λ) of 0.55 and residual CO_2 saturation (S_{gr}) of 0.25 result the in highly interfering behavior reported by Gran et al. (2017) while maintaining plausible reservoir injectivity. Figure 1 presents the complete parameter set for the relative permeability and capillary pressure models used for this study.

The code selection for this study is TOUGH3 (Jung et al., 2017) compiled with the ECO2N fluid property module (Pruess, 2005b), which updates the well-known TOUGH2 simulation code (Pruess et al., 1999) to implement PetSc (Balay et al., 2018) parallel solvers and includes gravitational potential in the energy balance. TOUGH3 solves energy and mass conservation equations for nonisothermal, multiphase flows in a porous geologic media. The ECO2N module simulates mixtures of H_2O, NaCl, and CO_2 for pressures up to 60 MPa, temperature between 10 and 110 °C, and salinity up to full halite saturation. The ECO2N module accounts for phase partitioning between water, CO_2, and NaCl on the basis of equilibrium solubility constraints (Pruess, 2005b).

4 Results and Discussion

The ensemble of 1-D homogeneous simulations reveal that the thermal fluid signature in a CCS reservoir is characterized by three distinct features: (1) a warming front at the leading edge of the CO_2 plume, (2) a zone of thermal equilibrium in the central portion of the CO_2 plume, and (3) a cooling zone near the injection well. Figure 2a presents a schematic illustration of these characteristic thermal features for a single 1-D realization after 20 years of injection. Figure 2b shows that permeability and porosity combinations vary the spatial dimensions of each thermal zone, as well as the magnitude of temperature change, but the overall pattern is independent of reservoir properties.

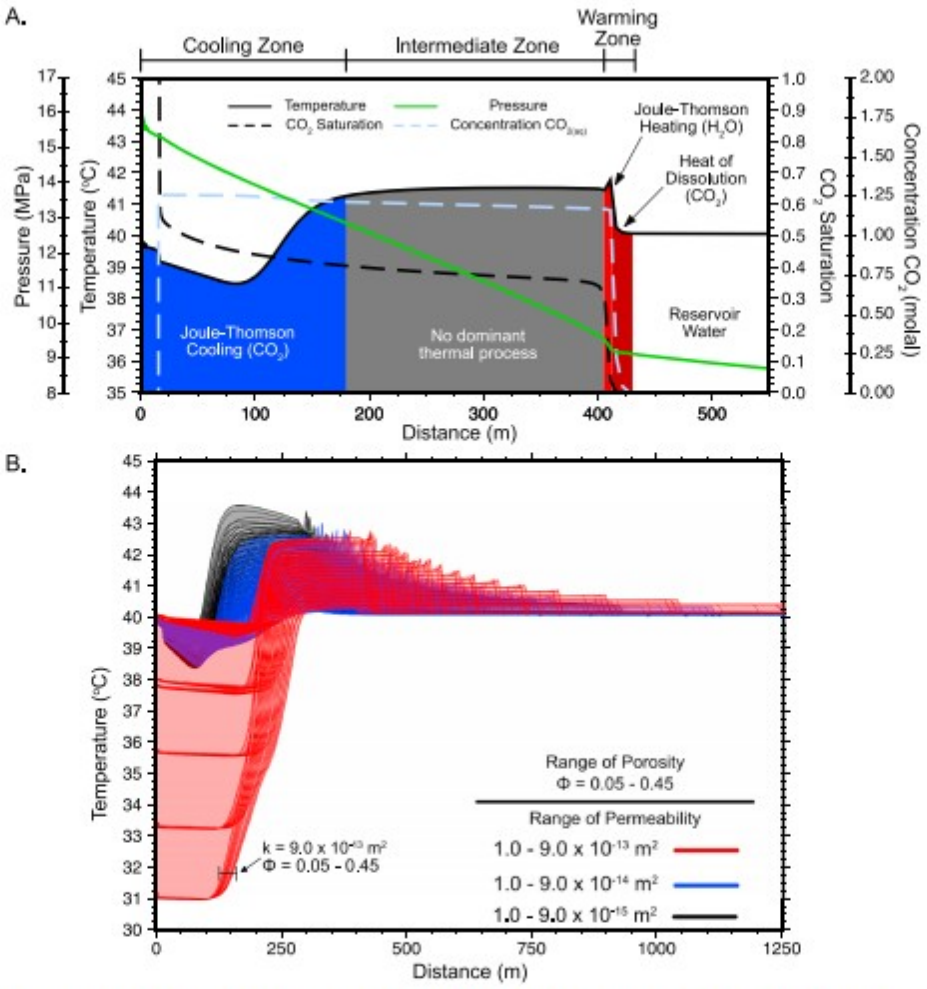

Figure 2. (a) Schematic illustration of the characteristic 1-D thermal profile after 20 years of injection for a single realization within the complete ensemble ($k = 8.0 \times 10^{-15}$ m^2, $\phi = 0.25$). Shading below the temperature curve (solid black line) denotes each thermal zone; dashed black line is CO_2 saturation, dashed blue line is dissolved CO_2 concentration, and solid green line is fluid pressure. (b) Temperature profiles for the complete 1-D simulation ensemble ($N = 459$) after 20 years of a constant mass CO_2 injection. Results are colored by permeability magnitude.

At the leading edge of the CO_2 plume, two different thermal fluid processes cause a distinct warming front to develop (Figure 2a, red shading). First, CO_2 dissolution into the reservoir water increases fluid temperature (heat of dissolution) as illustrated in Figure 2a by the contemporaneous arrival of increasing temperature and aqueous phase CO_2. Second, Joule-Thomson heating due to the expansion of water causes a small, but sharp temperature spike, which is illustrated in Figure 2a at ~415 m. This sharp thermal spike is caused by the reservoir water experiencing a rapid pressure drop between 405 and 415 m (Figure 2a, green line), which produces ~0.1 °C increase over a drop in pressure of 0.5 MPa and results in μ_{JT} of ~0.2 °C/MPa. While this increase in temperature is minimal, larger pressure drops caused during a CO_2 injection can result in a more significant temperature increase. The presence of Joule-Thomson heating is in agreement with the laboratory, and

numerical experiments of Zhang et al. (2018b) that show a pressure drop of 5 MPa causes a +1.1 °C temperature change during fluid circulation in an EGS system. This thermal anomaly corresponds with a μ_{JT} of ~0.2 °C/MPa and closely matches the results presented here.

Closer to the injection well, a zone of cooling develops where the expansion of CO_2 consumes thermal energy and the water is fully saturated with respect to CO_2, thus precluding the competing effect of dissolution heating (Figure 2a, blue shading). As a result, the thermal fluid signature near the injection well is characterized by a pronounced temperature depression. The central portion of the CO_2 plume is characterized by a zone of thermal equilibrium where (i) CO_2 is no longer expanding, so Joule-Thomson cooling does not occur, (ii) dissolution heating is no longer occurring because the reservoir water is saturated with respect to CO_2, and (iii) the pressure gradient is too low for water expansion, which precludes Joule-Thomson warming (Figure 2a, gray shading). Nevertheless, the effects of the warming front are persistent and the fluid temperature remains above background conditions until the near-well zone of cooling.

The complete simulation ensemble shows that the zonal temperature pattern discussed above occurs regardless of permeability and porosity; however, its lateral dimension and magnitude appear to scale with variations in hydraulic properties (Figure 2b). For the CCS scenario considered here, the maximum temperature increase at the warming front is 3.8 °C, while the maximum temperature depression in the cooling zone is 8.9 °C. To the first order, permeability governs the maximum lateral extent of CO_2 migration, and thus controls the radial extent of the thermal fluid signature. However, the magnitude of temperature change at the warming front appears to increase with higher porosity because additional pore space increases the fluid mass available for dissolution heating. In contrast, the thermal fluid signature of low-porosity cases is governed by the thermal contribution of the rock matrix, which keeps the fluid temperature closer to equilibrium with the surrounding reservoir (Han et al., 2010; Oldenburg, 2007). Within the warming front, these results also show that the temperature spike caused by water expansion increases as bulk permeability decreases (Figure 2b) because lower permeability increases the pressure gradient at the leading edge of the CO_2 plume. Moreover, CO_2 solubility in water also increases with increasing pressure (Carroll et al., 1991), so the maximum temperature increase occurs in the low-permeability scenarios (Figure 2b, black), while low temperatures tend to occur in the high-permeability scenarios (Figure 2b, red). Interestingly, phase interference between CO_2 and water can also drive pressure gradients at the leading edge of the CO_2 plume (Pollyea, 2016). Recent numerical studies show that relative permeability effects may cause variability in CO_2 injection pressure (Pollyea, 2016; Yoshida et al., 2016). For example, Pollyea (2016) utilizes numerical simulations to study how the uncertainty associated with relative permeability can affect a CO_2 injection. This study shows that for a constant mass CO_2 injection, maximum

injection pressure can vary from 5–60 MPa over a range of van Genuchten parameters. This wide range of injection pressures caused by varying relative permeability parameters suggests that relative permeability effects may be an important contributor to the thermal fluid signature of CCS operations.

Near the injection well, the ensemble results also show that Joule-Thomson cooling is most pronounced for the cases with high reservoir permeability (Figure 2b, red). This is the result of salt precipitation near the injection well (salting-out), which fills pore space, decreases permeability, and causes steep pressure gradients to develop in the near-well region (Zhao & Cheng, 2017). These sharp pressure gradients cause the CO_2 to expand rapidly as it migrates beyond the near-well region, which for this study results in a maximum temperature drop of ~9 °C due to Joule-Thomson cooling effects. In fact, Oldenburg (2007) found that Joule-Thomson cooling can account for 20 °C temperature drop when CO_2 is injected into natural gas reservoirs.

The 1-D simulation ensemble reveals a characteristic pattern in the radial dimension of fluid temperature during CCS operations. To investigate the vertical dimension, we discretized a single simulation grid into 2-m vertical segments, resulting in a 2-D, radially symmetric, and homogeneous reservoir model. Results from this 2-D simulation are presented as a time series in Figure 3 and show that the CO_2 plume and warming front migrate contemporaneously throughout the thickness of the reservoir. The vertical temperature distribution is governed by the shape of the CO_2 plume, which is controlled by a combination of capillary and buoyancy forces (Wu et al., 2018); however, the characteristic thermal structure illustrated by the 1-D models is still prevalent in Figure 3 irrespective of depth. As the CO_2 migrates further into the reservoir the heat produced by CO_2 dissolution and Joule-Thomson warming migrates with the CO_2 plume and reservoir water, while the zone of cooling expands radially from the injection well. These results are similar to those of Han et al. (2012), where they show that the dissolution of CO_2 into the reservoir water results in a 1–5 °C temperature increase and this maximum temperature increase corresponds to the interface between the CO_2 and reservoir water.

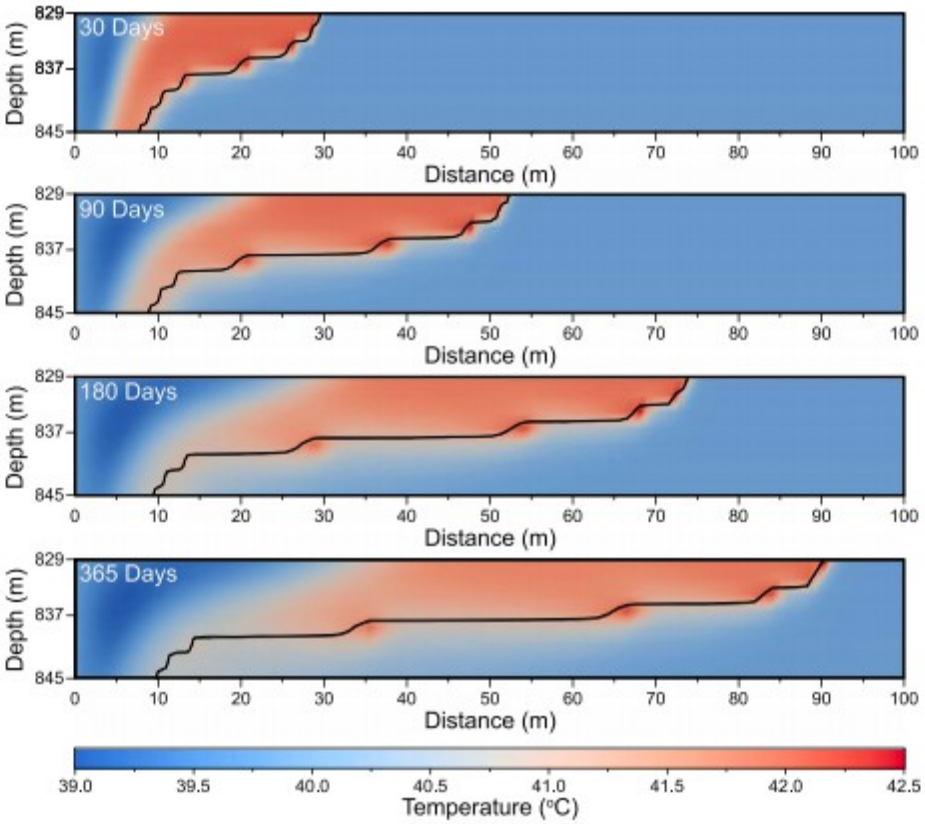

Figure 3. Temporal evolution of CO_2 saturation and temperature for 2-D simulation with the same hydraulic reservoir properties as Figure 2a. Each panel is colored by reservoir temperature and 1% CO_2 is contoured as a solid black line. Note that 1% CO_2 saturation and the maximum temperature within the reservoir move contemporaneously through time.

The 1-D and 2-D model results discussed above reveal that an advancing CO_2 plume is accompanied in space and time by a positive thermal anomaly at its leading edge. This result is discordant with a recent study by Jayne et al. (2019), which found that the positive thermal anomaly advances ahead of the CO_2 plume in a highly heterogeneous basalt reservoir. While Jayne et al. (2019) suggested that thermal monitoring may be an effective strategy for heterogeneous reservoirs, they did not provide a mechanistic explanation. As a result, we further analyzed a simulation from Jayne et al. (2019) to make the mechanistic connection between the temperature distribution in a heterogeneous reservoir and the thermodynamic processes responsible for the thermal signature discussed above. Figure 4a shows the isosurface contour for 1% CO_2 saturation in a synthetic Columbia River Basalt reservoir with a spatially correlated (Jayne & Pollyea, 2018), but randomly generated, permeability field. The CO_2 plume is shaded by change in temperature from pre-injection to post-injection and shows a positive thermal signature of up to 3.5 °C at the edges of the CO_2. This is clearly the same phenomenon revealed by the 1-D simulations that show a warming front governed by heat of dissolution and water expansion. Moreover, by interrogating stream tubes showing the direction of heat flow, we find that heat is migrating laterally

ahead of the CO_2 plume and vertically into the confining layer (Figure 4b, detail section).

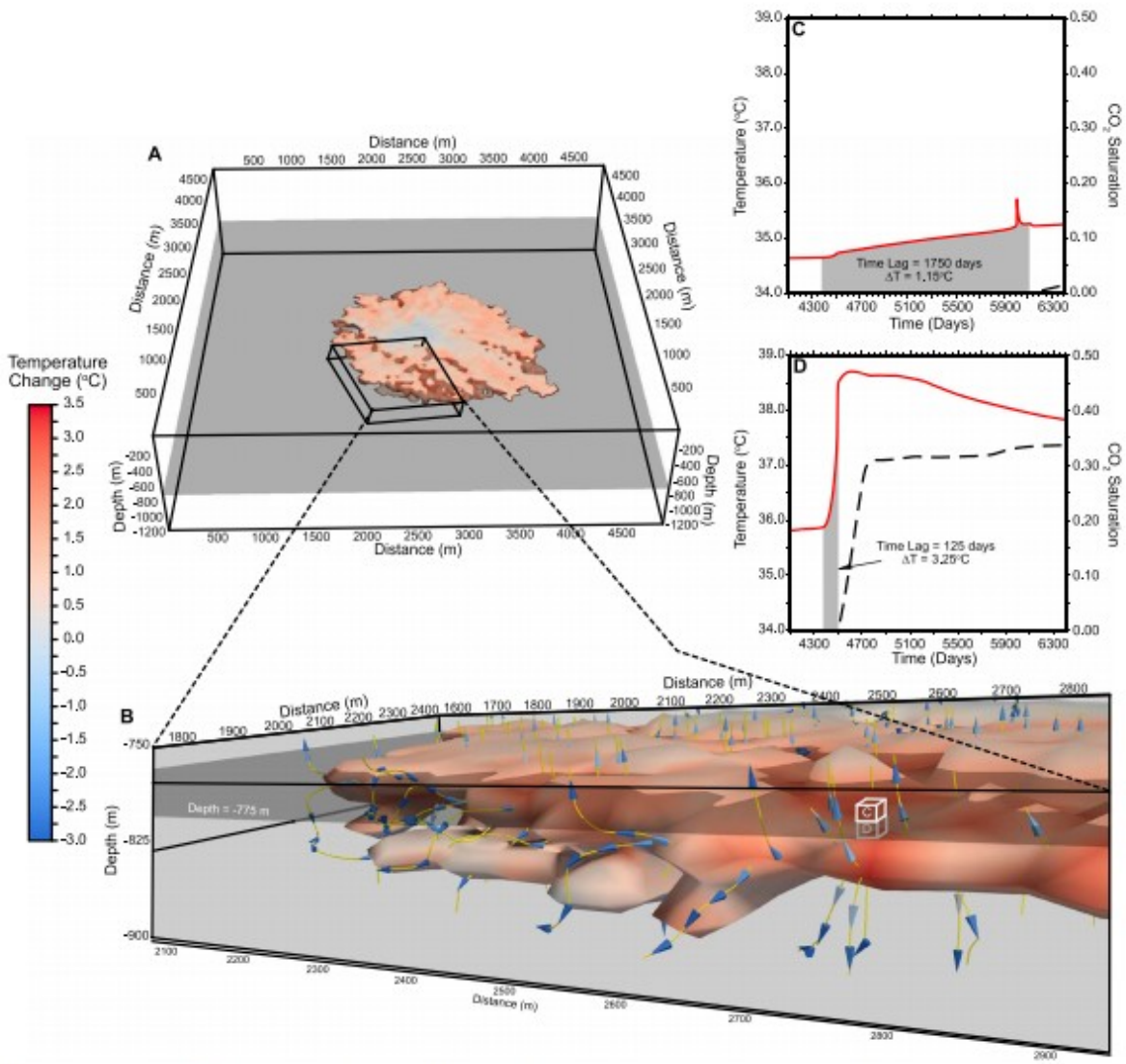

Figure 4. A single realization from Jayne et al. (2019), Panel (a) shows the isosurface for 1% CO_2 saturation after 15 years of a CO_2 injection and is contoured by temperature. (b) A subsection of the CO_2 plume is shown along with stream tubes indicating the direction of heat flow. The layer of gray shading corresponds to the boundary between the storage reservoir and overlying caprock. (c and d) Two plots of temperature (red line) and CO_2 saturation (black line) versus time are shown for two grid blocks 400 m away from the injection well; panel (c) represents a grid block in the entablature zone, panel (d) is a grid block within the injection zone.

To test temperature monitoring as predictor of CO_2 breakthrough, we reproduced the 3-D basalt CCS simulation developed by Jayne et al. (2019) and recorded time series temperature data for two adjacent grid cells located 400 m from the injection well: Cell C is within the caprock overlying the reservoir and cell D is within the reservoir (Figure 4, detail section). These results show that within the injection zone temperature begins increasing 125 days before the arrival of the CO_2 plume (Figure 4d).

However, there is a 1,750-day time lag between temperature change and free-phase CO_2 arrival within the caprock overlying the reservoir (Figure 4c). Within each grid cell temperature increases steadily until the maximum temperature is reached with the arrival of free-phase CO_2. The difference in time lag between the reservoir and caprock is explained by the permeability differences between them. However, the presence of the time lag itself is markedly different than what is observed for homogeneous reservoirs. The time lag can be reasonably explained by relative permeability effects in the presence of heterogeneous permeability fields (Pollyea & Fairley, 2012). Specifically, the positive thermal anomaly associated with heat of dissolution begins when CO_2 dissolves into the aqueous phase. At the leading edge of the CO_2 plume this process occurs at relatively low free-phase CO_2 saturation. As a result, aqueous (wetting) phase mobility is much higher than the nonwetting phase, so the aqueous phase can migrate further into the reservoir under the same pressure gradient. This results in advective transport of the thermal mass ahead of the trailing CO_2 plume (Figure 4, detail section), and the effects become more pronounced as heterogeneous permeability fields facilitate the development of preferential flow paths.

5 Conclusions

This study illustrates that thermal effects associated with CCS operations can result in significant temperature changes within and beyond the reservoir. We find that these temperature changes may be a cost-effective and readily implemented monitoring tool during CCS operations in highly heterogeneous reservoirs. This study implements a numerical modeling experiment to compare the thermal fluid signature that develops during CO_2 injection within homogeneous and heterogeneous geologic reservoirs. The findings from this study are as follows:

1. The thermodynamic processes of Joule-Thomson heating and cooling combined with heat of dissolution result in a characteristic thermal profile in homogeneous reservoirs.
2. At the leading edge of a CO_2 plume, the combination of heat of dissolution and Joule-Thomson heating (H_2O expansion) causes reservoir temperatures to increase up to 4 °C.
3. Joule-Thomson cooling (CO_2 expansion) causes reservoir temperatures to decrease as much as 9 °C near a CO_2 injection well.
4. In homogeneous reservoirs increased reservoir temperatures due to heat of dissolution and Joule-Thomson heating migrate concurrently through the reservoir, suggesting temperature could be a proxy for CO_2 breakthrough.
5. In highly heterogeneous reservoirs CO_2 injections result in a much more complex thermal structure where increased reservoir temperatures can arrive within a monitoring well weeks before the arrival of a free-phase CO_2.

In conclusion, results from this study yield important insights into the thermal processes taking place within a CO_2 plume during a CO_2 injection scenario. The heat of dissolution and Joule-Thomson effects of both CO_2 and water cause a temporally and spatially evolving thermal profile within the storage reservoir. The combination of simplified 1-D homogeneous simulations with complex heterogeneous 3-D simulations yield important guidance in the application of temperature monitoring as a predictor of CO_2 breakthrough in CCS operations.

Acknowledgments

We thank Curt Oldenburg for insightful discussions about thermal fluid processes in the CO_2-water system. We also thank Philip Stauffer and one anonymous reviewer for their thorough reviews of an early draft of this manuscript. This study received financial support from the U.S. Department of Energy National Energy Technology Laboratory through cooperative agreement DE-FE0023381 (PI Pollyea). All data analyzed as part of this study were produced with the TOUGH3 numerical simulation code (Jung et al., 2017), which is publicly available from Lawrence Berkeley National Laboratory. Input files for each simulation are available within the supporting information.

References

Anderson, T. R., & Fairley, J. P. (2008). Relating permeability to the structural setting of a fault-controlled hydrothermal system in southeast Oregon, USA. *Journal of Geophysical Research*, 113, B05402. https://doi.org/10.1029/2007JB004962

André, L., Azaroual, M., & Menjoz, A. (2010). Numerical simulations of the thermal impact of supercritical CO_2 injection on chemical reactivity in a carbonate saline reservoir. *Transport in porous media*, 82(1), 247– 274.

Bachu, S. (1988). Analysis of heat transfer processes and geothermal pattern in the Alberta Basin, canada. *Journal of Geophysical Research*, 93(B7), 7767– 7781.

Balay, S., Abhyankar, S., Adams, M. F., Brown, J., Brune, P., Buschelman, K., Dalcin, L., Dener, A., Eijkhout, V., Gropp, W. D., Kaushik, D., Knepley, M. G., May, D. A., McInnes, L. C., Mills, R. T., Munson, T., Rupp, K., Sanan, P., Smith, B. F., Zampini, S., Zhang, H., & Zhang, H. (2018). PETSc users manual (*Tech. Rep. ANL-95/11 - Revision 3.10*): Argonne National Laboratory. http://www.mcs.anl.gov/petsc

Bodvarsson, G. (1969). On the temperature of water flowing through fractures. *Journal of Geophysical Research*, 74(8), 1987– 1992.

Carroll, J. J., Slupsky, J. D., & Mather, A. E. (1991). The solubility of carbon dioxide in water at low pressure. *Journal of Physical and Chemical Reference Data*, 20(6), 1201– 1209.

Conant, B. Jr (2004). Delineating and quantifying ground water discharge zones using streambed temperatures. *Groundwater*, 42(2), 243– 257.

Engel, T., & Reid, P. J. (2010). *Thermodynamics, statistical thermodynamics, and kinetics*. NJ, USA: Prentice Hall Upper Saddle River.

Gran, M., Zahasky, C., Garing, C., Pollyea, R., & Benson, S. (2017). Core-flooding experiments combined with X-rays and micro-PET imaging as a tool to calculate fluid saturations in a fracture. Fall Meeting of the American Geophysical Union, Abstract H21C-1466.

Han, W. S., Kim, K.-Y., Park, E., McPherson, B. J., Lee, S.-Y., & Park, M.-H. (2012). Modeling of spatiotemporal thermal response to CO_2 injection in saline formations: interpretation for monitoring. *Transport in porous media*, 93(3), 381– 399.

Han, W. S., Stillman, G. A., Lu, M., Lu, C., McPherson, B. J., & Park, E. (2010). Evaluation of potential nonisothermal processes and heat transport during CO_2 sequestration. *Journal of Geophysical Research*, 115, B07209. https://doi.org/10.1029/2009JB006745

Heffner, J., & Fairley, J. (2006). Using surface characteristics to infer the permeability structure of an active fault zone. *Sedimentary Geology*, 184(3-4), 255– 265.

Hurter, S., Garnett, A. A., Bielinksi (Statoil), A., & Kopp, A. (2007). Thermal signature of free-phase CO_2 in porous rocks: Detectability of CO_2 by temperature logging. In *Offshore europe*, Society of Petroleum Engineers, Scotland, U.K.

Jayne, R. S., Hao, W., & Pollyea, R. M. (2019). Geologic CO_2 sequestration and permeability uncertainty in a highly heterogeneous reservoir. *International Journal of Greenhouse Gas Control*, 83, 128– 139.

Jayne, R. S., & Pollyea, R. M. (2018). Permeability correlation structure of the Columbia River plateau and implications for fluid system architecture in continental large igneous provinces. *Geology*, 46(8), 715– 718.

Jung, Y., Pau, G. S. H., Finsterle, S., & Pollyea, R. M. (2017). TOUGH3: A new efficient version of the TOUGH suite of multiphase flow and transport simulators. *Computers & Geosciences*, 108, 2– 7.

King, A. D. Jr, & Coan, C. (1971). Solubility of water in compressed carbon dioxide, nitrous oxide, and ethane. Evidence for hydration of carbon dioxide and nitrous oxide in the gas phase. *Journal of the American Chemical Society*, 93(8), 1857– 1862.

Koschel, D., Coxam, J.-Y., Rodier, L., & Majer, V. (2006). Enthalpy and solubility data of CO_2 in water and NaCl(aq) at conditions of interest for geological sequestration. *Fluid phase equilibria*, 247(1-2), 107– 120.

Lee, D. R. (1985). Method for locating sediment anomalies in lakebeds that can be caused by groundwater flow. *Journal of Hydrology*, 79(1-2), 187– 193.

Manga, M. (2001). Using springs to study groundwater flow and active geologic processes. *Annual Review of Earth and Planetary Sciences*, 29(1), 201– 228.

Mathias, S. A., Gluyas, J. G., de Miguel, G. J. G. M., Bryant, S. L., & Wilson, D. (2013). On relative permeability data uncertainty and CO_2 injectivity estimation for brine aquifers. *International Journal of Greenhouse Gas Control*, 12, 200– 212.

Matter, J. M., Stute, M., Snæbjörnsdottir, S. O., Oelkers, E. H., Gislason, S. R., Aradottir, E. S., Sigfusson, B., Gunnarsson, I., Sigurdardottir, H., Gunnlaugsson, E., Axelsson, G., Alfredsson, H. A., Wolff-Boenisch, D., Mesfin, K., de la Reguera Taya, D. F., Hall, J., Dideriksen, K., & Broecker, W. S. (2016). Rapid carbon mineralization for permanent disposal of anthropogenic carbon dioxide emissions. *Science*, 352(6291), 1312– 1314.

McGrail, B. P., Schaef, H. T., Spane, F. A., Cliff, J. B., Qafoku, O., Horner, J. A., Thompson, C. J., Owen, A. T., & Sullivan, C. E. (2017). Field validation of supercritical CO_2 reactivity with basalts. *Environmental Science & Technology Letters*, 4(1), 6– 10.

NIST (2018). Thermophysical properties of fluid systems. Retrieved from http://webbook.nist.gov/chemistry/fluid/ (access on 7 May 2019).

Oldenburg, C. M. (2007). Joule-Thomson cooling due to CO_2 injection into natural gas reservoirs. *Energy Conversion and Management*, 48(6), 1808– 1815.

Pollyea, R. M. (2016). Influence of relative permeability on injection pressure and plume configuration during CO_2 injections in a mafic reservoir. *International Journal of Greenhouse Gas Control*, 46, 7– 17.

Pollyea, R. M., & Fairley, J. P. (2012). Implications of spatial reservoir uncertainty for CO_2 sequestration in the east Snake River Plain, Idaho (USA). *Hydrogeology Journal*, 20(4), 689– 699.

Pruess, K. (2005a). Numerical studies of fluid leakage from a geologic disposal reservoir for CO_2 show self-limiting feedback between fluid flow and heat transfer. *Geophysical research letters*, 32, L14404. https://doi.org/10.1029/2005GL023250

Pruess, K. (2005b). *ECO2N: A TOUGH2 fluid property module for mixtures of water, NaCl, and CO_2*. Berkeley, CA: Lawrence Berkeley National Laboratory.

Pruess, K., & Doughty, C. (2010). Thermal single-well injection-withdrawal tracer tests for determining fracture-matrix heat transfer area (*Tech. rep.*) Berkeley, CA (United States): Lawrence Berkeley National Lab.(LBNL).

Pruess, K., Oldenburg, C., & Moridis, G. (1999). TOUGH2 user's guide, Version 2 (*Tech. rep., LBNL-43134*): Lawrence Berkeley National Laboratory.

Roebuck, J., Murrell, T., & Miller, E. (1942). The Joule-Thomson effect in carbon dioxide. *Journal of the American Chemical Society*, 64(2), 400– 411.

Shook, G. M., & Suzuki, A. (2017). Use of tracers and temperature to estimate fracture surface area for EGS reservoirs. *Geothermics*, 67, 40– 47.

Slichter, C. S. (1905). Field measurements of the rate of movement of underground waters. *United States Geological Survey Water-Supply and Irrigation Paper*, 140, 172.

Stauffer, P. H., Lewis, K., Stein, J. S., Travis, B. J., Lichtner, P., & Zyvoloski, G. (2014). Joule–Thomson effects on the flow of liquid water. *Transport in porous media*, 105(3), 471– 485.

Storey, R. G., Howard, K. W., & Williams, D. D. (2003). Factors controlling riffle-scale hyporheic exchange flows and their seasonal changes in a gaining stream: A three-dimensional groundwater flow model. *Water Resources Research*, 39(2), 1034. https://doi.org/10.1029/2002WR001367

Van Genuchten, M. (1980). A closed-form equation for predicting the hydraulic conductivity of unsaturated soils. *Soil Science Society of America*, 44, 892– 898.

Wu, H., Jayne, R. S., & Pollyea, R. M. (2018). A parametric analysis of capillary pressure effects during geologic carbon sequestration in a sandstone reservoir. *Greenhouse Gases: Science and Technology*, 8(6), 1039– 1052.

Yoshida, N., Levine, J. S., & Stauffer, P. H. (2016). Investigation of uncertainty in CO_2 reservoir models: A sensitivity analysis of relative permeability parameter values. *International Journal of Greenhouse Gas Control*, 49, 161–178.

Zeidouni, M., Nicot, J.-P., & Hovorka, S. D. (2014). Monitoring above-zone temperature variations associated with CO_2 and brine leakage from a storage aquifer. *Environmental earth sciences*, 72(5), 1733– 1747.

Zhang, Y., Doughty, C., Pan, L., Kneafsey, T., and the EGS Collab Team. –EGS Collab Team authorship: Ajo-Franklin, J., Bauer, S. J., Baumgartner, T., Beckers, K., Blankenship, D., Bonneville, A., Boyd, L., Brown, S. T., Burghardt, J. A., Chen, T., Chen, Y., Condon, K., Cook, P. J., Dobson, P. F., Doe, T., Doughty, C. A., Elsworth, D., Feldman, J., Foris, A., Frash, L. P., Frone, Z., Fu, P., Gao, K., Ghassemi, A., Gudmundsdottir, H., Guglielmi, Y., Guthrie, G., Haimson, B., Hawkins, A., Heise, J., Herrick, C. G., Horn, M., Horne, R. N., Horner, J., Hu, M., Huang, H., Huang, L., Im, K., Ingraham, M., Johnson, T. C., Johnston, B., Karra, S., Kim, K., King, D. K., Kneafsey, T., Knox, H., Knox, J., Kumar, D., Kutun, K., Lee, M., Li, K., Lopez, R., Maceira, M., Makedonska, N., Marone, C., Mattson, E., McClure, M. W., McLennan, J., McLing, T., Mellors, R. J., Metcalfe, E., Miskimins, J., Morris, J. P., Nakagawa, S., Neupane, G., Newman, G., Nieto, A., Oldenburg, C. M., Pan, W., Pawar, R., Petrov, P., Pietzyk, B., Podgorney, R., Polsky, Y., Porse, S., Richard, S., Robertson, M., Roggenthen, W., Rutqvist, J., Rynders, D., Santos-Villalobos, H., Schwering, P., Sesetty, V., Singh, A., Smith, M. M., Sone, H., Strickland, C. E., Su, J.,

Ulrich, C., Uzunlar, N., Vachaparampil, A., Valladao, C. A., Vandermeer, W., Vandine, G., Vardiman, D., Vermeul, V. R., Wagoner, J. L., Wang, H. F., Weers, J., White, J., White, M. D., Winterfeld, P., Wood, T., Wu, H., Wu, Y. S., Wu, Y., Zhang, Y., Zhang, Y. Q., Zhou, J., Zhou, Q., & Zoback, M. D. (2018b). What could we see at the production well before the thermal breakthrough? In *Proceedings, 43rd Workshop on Geothermal Reservoir Engineering*, Stanford University.

Zhang, Y., Freifeld, B., Finsterle, S., Leahy, M., Ennis-King, J., Paterson, L., & Dance, T. (2011). Estimating CO_2 residual trapping from a single-well test: Experimental design calculations. *Energy Procedia*, 4, 5044– 5049.

Zhang, Y., Jung, Y., Freifeld, B., & Finsterle, S. (2018a). Using distributed temperature sensing to detect CO_2 leakage along the injection well casing. *International Journal of Greenhouse Gas Control*, 74, 9– 18.

Zhao, R., & Cheng, J. (2017). Effects of temperature on salt precipitation due to formation dry-out during CO_2 injection in saline aquifers. *Greenhouse Gases: Science and Technology*, 7(4), 624– 636.